Heliyon 7 (2021) e07058

Contents lists available at ScienceDirect

Heliyon

journal homepage: www.cell.com/heliyon

Research article

Synthesis and fabrication of films including graphene oxide functionalized with chitosan for regenerative medicine applications

Ana María Valencia [a], Carlos Humberto Valencia [b], Fabio Zuluaga [a], Carlos David Grande-Tovar [c,*]

[a] Laboratorio SIMERQO Polímeros, Departamento de Química, Universidad del Valle, Calle 13 # 100-00, Cali 76001, Colombia
[b] Escuela de Odontología, Grupo Biomateriales Dentales, Universidad del Valle, Calle 4B No. 36-00, Cali 76001, Colombia
[c] Grupo de Investigación de Fotoquímica y Fotobiología, Universidad del Atlántico, Carrera 30 Número 8-49, Puerto Colombia 081008, Colombia

ARTICLE INFO

Keywords:
Chitosan
Graphene oxide
Regenerative medicine
Tissue engineering

ABSTRACT

Graphene oxide (GO) has recently gained attention as a scaffold reinforcing agent for tissue engineering. Biomechanical and biological properties through a synergistic effect can be strengthened when combined with other materials such as chitosan (CS). For that reason, chitosan was used for Graphene Oxide (GO) functionalization through an amide group whose formation was evident by bands around 1600 cm^{-1} in the FTIR analysis. Furthermore, bands located at 1348 cm^{-1} (D band), 1593 cm^{-1} (G band), and 2416 cm^{-1} (2D band) in the RAMAN spectrum, and the displacement of the signal at 87.03 ppm (C5) in solid-state ^{13}C-NMR confirmed the amide formation. Films including the CS-GO compound were prepared and characterized by thermogravimetric analysis (TGA), where CS-GO film presented a lighter mass loss (~10% less loosed) than CS due probably to the covalent functionalization with GO, providing film thermal resistance. The CS-GO films synthesized were implanted in Wistar rats' subdermal tissue as a first approximation to the biological response. In vivo tests showed a low inflammatory response, good cicatrization, and advanced resorption at 60 days of implantation, as indicated by histological images. It was evidenced that the covalent union between CS and GO increased biocompatibility and the degradation/resorption capacity, demonstrating tissue regeneration with typical characteristics and tiny remnants of implanted material surrounded by a type III collagen capsule. These results show the potential application of the new synthesized films, including the CS-GO compound, in tissue engineering.

1. Introduction

The high requirement for tissue and organ transplantations and their low availability have created a global health concern [1]. From the engineering area, the use of biomaterials for synthetic scaffolds restoring specific tissues has been proposed as a safe and secure alternative.

The main goal of bone tissue engineering is to repair a bone defect without an allograft or an autograft [2]. This way, the scaffold fulfills the function of guiding bone neoformation, serving as a support for bone cells.

However, one of the biggest challenges in bone tissue regeneration is to provide porosity in the scaffold that can mimic the physical and chemical properties of the extracellular matrix and can support cell adhesion and proliferation [3].

Biopolymers are versatile materials that can be safely used in the human body [4], allowing replacing different tissues based on their biocompatibility. One of the most used biopolymers in tissue engineering is chitosan (CS), a chitin derivate with glucosamine and N-acetyl glucosamine units linked by β-(1,4) bonds [5].

Through the years, CS has gained popularity in different areas, especially in tissue engineering, due to its excellent properties such as antimicrobial activity, biocompatibility, and high degradability rate, which do not produce an exaggerated inflammatory response [6, 7]. The cationic nature of CS also allows the interaction with negative charge components present in extracellular matrices such as amino glycans and glycosaminoglycans, improving the biological interaction and fixation in the body tissues [8].

CS has been combined with different polymeric and inorganic compounds for scaffold fabrication, designed to have similar properties to the extracellular matrix, which provides an optimum cellular growth environment. CS presents poor mechanical properties due to a high-water affinity, leading to quick deterioration. Therefore, numerous methods for improving CS mechanical properties [9] have been reported in the latest years. The use of pristine carbon materials such as carbon

* Corresponding author.
E-mail address: carlosgrande@mail.uniatlantico.edu.co (C.D. Grande-Tovar).

https://doi.org/10.1016/j.heliyon.2021.e07058
Received 22 July 2020; Received in revised form 8 November 2020; Accepted 10 May 2021

nanotubes [10], nano-onions [11, 12], graphene [13], and graphene oxide [14, 15] has gained popularity, and CS has been linked to overcoming the drawbacks of low mechanical properties [16].

Graphene oxide (GO) is a very resistant two-dimensional structure consisting of sheets of a carbon atom thickness obtained from graphite oxidation [17], which improves solubility and, consequently, provides a broad range of applications [18]. Besides its biocompatibility and large surface area, GO is an ideal candidate for scaffold fabrication due to many oxygen groups that provide hydrophilicity and cell affinity [19]. Additionally, GO can improve cell adhesion and induce stem cell differentiation to osteoblasts [20].

Chemical functionalization of CS and GO has been carried out for multiple applications such as wound healing [21, 22], cartilage, and bone regeneration [23], among others [24]. However, to the best of our knowledge, only a few reports for in vivo evaluation of tissue engineering applications are known. Our group previously reported scaffolds based on physical mixtures of CS and GO [25].

For the above reasons, in the present study, we covalently functionalized GO with CS (CS-GO) and prepared films to evaluate the biocompatibility using *in vivo* implantations in subdermal tissue for 60 days. The excellent film's biocompatibility obtained demonstrated the scaffold's potential use in tissue regeneration.

2. Materials and methods

GO synthesis followed the modified Hummer-Offemann method previously reported [26]. For the GO functionalization, chitosan with a deacetylation degree of 58% and a molecular weight (Mw) of 15323 Da reacted with GO. Gel Permeation Chromatography measured CS molecular weight using an Agilent 1260 instrument (Agilent Technologies, Santa Clara, CS, USA) equipped with an RI detector and two- Shodex column system using a flow rate of 0.5 mL/min. An Mw calibration curved using pullulan standards was employed.

For the GO functionalization, 1g of CS and 50 mg of GO were dispersed in a flask with 50 mL of dimethylformamide (Merck KGaA, Darmstadt, Germany). The mixture was introduced in ultrasound equipment for an hour, followed by the addition of 0.45 g (0.21 mmol) of dicyclohexilcarbodiimide (Merck KGaA, Darmstadt, Germany) and 0.3 g (2.45 mmol) of dimethylaminopyridine (Merck KGaA, Darmstadt, Germany). The mixture was left to stand for 48 h at room temperature, and the solid formed was isolated by centrifugation then washed three times with 50 mL of Milli Q water, 50 mL of methanol (Merck KGaA, Darmstadt, Ger-many), and 50 mL of acetone (Sigma-Aldrich, Palo alto, CA, USA), and dried at 60 °C for 24 h [22, 24].

GO and CS-GO were characterized by Raman spectroscopy using a confocal Raman microscope (Renishaw InVia Reflex, Wotton-under-Edge, UK) in a 1000-3000 cm^{-1} range. Sample absorption bands were analyzed by infrared spectroscopy using a Fourier Affinity-1 transform infrared spectrophotometer (Shimadzu, Kyoto, Japan) in a 500-4000 cm^{-1} range. The carbon nucleus present in the samples was identified by nuclear magnetic resonance in a Bruker Ultra Shield 400 MHz NMR equipment in solid-state mode.

CS, CS-GO, and the physical mixture of CS and GO (CS/GO) films were prepared using a previously reported methodology (Biranje S. et al., (2017). Briefly, five milligrams of each compound (CS, CS-GO, and CS/GO) were taken and dissolved in a 2.0% (v/v) acetic acid solution with constant stirring. Subsequently, glycerol was added as a plasticizer in a 2.5% (v/v) and stirred for 30 min until the polymer was completely dissolved. Finally, the dispersion was placed on acetate support and dried at room temperature for 24 h until solvent evaporated, then went to dry in an oven at 40 °C for an additional 24h period [27].

Thermal analyzes of CS, GO, and CS-GO films were performed using a TA instruments 2050 thermobalance, under a continuous nitrogen gas (90 mL/min) flow. The samples were heated up to 700 °C at a heating rate of 10 °C/min. The sample weight was approximately 3.0 mg for each determination.

Biological *in vitro* tests (brine shrimp test and gingival fibroblasts cell growth) were performed to probe CS-GO biocompatibility.

Biological in vivo tests were performed following the ISO 10993 standards recommendation. Subdermal implantation tests were carried out in three stages. Three-four months old healthy male Wistar rats, supplied and certificated by the Labbio laboratory (Bioterio) from Universidad del Valle, were used as biomodels in each step. Murine specimens are universally utilized in biomaterial research due to the low cost, size, and easy manipulation, besides being highly standardized as biomodels.

For the tests, films of 1 cm × 0.5 cm and 2mm thickness were used. The first step consisted of 30 days of implantation using films of CS-GO and a collagen film as control. The second stage was performed for 60 days. CS-GO was implanted, and CS was used as a control to observe the organism's response to the implantation. The third stage was performed for 60 days, in which CS-GO was tested, and CS/GO (physical mixture) was used as a control sample.

In every case, samples were implanted into the dorsal subdermal area in defects of 1 cm large per 3 cm thickness. The preparation was closed with a silk 4/0 suture. Samples were recovered, fixed on a formaldehyde buffer, and washed with PBS (Phosphate buffer solution). Then, samples were decalcified for five days with a SHANDON TBD-2 Decalcifier (Thermo Fisher Scientific, Massachusetts, USA) and dehydrated in alcohol solutions of ascending concentration (70%, 80%, 95%, and 100%). Finally, the samples were diaphanized with xylol and infiltrated with paraffin for later cutting at 5 μm using a Thermo ScientificTM Histoplast™ (Thermo Fisher Scientific, Massachusetts, USA) and an Autotechnicon Tissue Processor™ (Leica Microsystems, Mannheim, Germany).

Ultimately, Masson's trichromacy analysis of samples to observe collagen type I and Gomori's trichromacy to observe Collagen type III was performed. The hematoxylin-eosin technique was used to monitor general tissue architecture. For analyzes, the images, a Leica DM750 microscope with a Leica DFC 295 camera and Leica Application Suite version 4.12.0 (Leica Microsystem, Mannheim, Germany) imaging software was used. The Universidad del Valle (Cali, Colombia) animal ethics review committee approved this research, according to the endorsement of ethics committee CEAS 001-016.

3. Results and discussion

GO is easily dispersed in polar solvents like DMF, leading to a loss of the GO stacks [28], necessary to facilitate the functionalization reaction between CS amino groups and oxygenated groups from GO. Their combination is considered a promising nanocomposite in tissue engineering [25] due to the synergistic effect between CS and GO with biological and mechanical reinforcement [19, 29].

CS forms a semi-rigid precipitate that can be processed into multiple forms as gels, beads, and films [30]. On the other hand, GO can improve the mechanical properties of the biocomposite and promote the adhesion and proliferation of osteoblasts [29]. In this way, the incorporation of GO into the CS matrix stabilizes the compound, improving mechanical and biological properties.

The Raman Spectrum (Figure 1) shows the characteristic bands for GO [31]. The D band is located at 1344 cm^{-1}, the G band at 1590cm^{-1}, and the 2D band at 2424 cm^{-1}. For the CS-GO compound, the D band is located at 1348 cm^{-1}, the G band at 1593 cm^{-1}, and the 2D band at 2416 cm^{-1}. Raman analysis indicated that both materials (GO and CS-GO) were grossly similar. According to Marcano (2010), all spectrum associated with GO presents the D and G bands [32]. López-Diaz (2017) evidenced that those bands are activated by a single-phonon intervalley and intravalley scattering processes [33]. Usually, the ratio between the D and G intensity bands (I_D/I_G) determines the degree of functionalization (disorder) [31] obtained. In the present case, the I_D/I_G was 0.845 for GO and 0.846 for CS-GO, meaning that a high density of defects was obtained [34]. The higher the ratio of 2D and G band (I_{2D}/I_G), the fewer

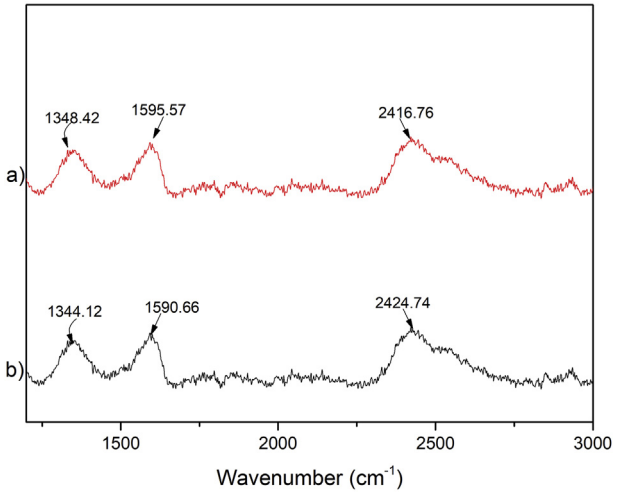

Figure 1. Raman characterization of a) CS-GO and b) GO compounds.

layers in the material [33]. The I_{2D}/I_G of single-layer graphene is generally above 2 [33]. The ratio obtained in the present study was 1.52 for GO and 1.51 for CS-GO, which means that both materials are multilayer.

The FTIR spectrum of GO shown in Figure 2a exhibits a band at 1628cm^{-1} corresponding to C=C skeletal vibration of the non-oxidized graphitic domain [24]. Bands at 3230 cm^{-1} (O–H stretching) and 1721cm^{-1} (C=O stretching) indicate carboxyl groups present in the structure, demonstrating a successful functionalization of the graphitic structure [35]. The band at 860 cm^{-1} corresponds to C=C's presence from the initial graphite [36], and the absorption band at 976 cm^{-1} corresponds to the C–O–C vibration. For CS (Figure 2b), characteristic bands were observed [18]. The stretching band of C–H at 2905 cm^{-1}, 1659, and 1592 cm^{-1} correspond to the amine I and II. The band observed at 1400cm^{-1} corresponds to the C–N stretching of the amine.

Figure 2c, the CS-GO spectrum shows a band at 1663 cm^{-1} due to the stretching vibration of C=O in the amide resulting from GO carboxyl groups (COOH), CS amine (NH_2) groups overlapping with the amine I band of CS. There is also an absorption band around 1010 and 1160 cm^{-1}, attributed to the primary alcoholic group of C_6–OH [37], according to Hal et al. (2011) [37]. The bands obtained for CS-GO are similar to the CS. According to Muda et al. (2020), the spectrum corresponding to this material should have a combination of characteristics [38]. The band

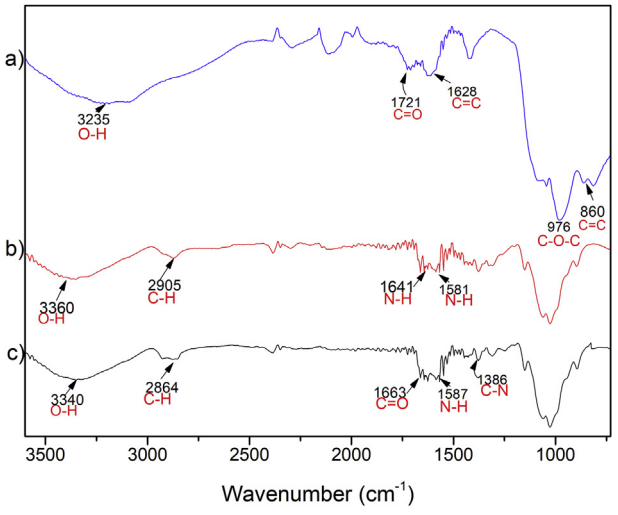

Figure 2. Fourier transform infrared spectroscopy (FTIR) characterization of a) GO, b) CS, and c) CS-GO.

at 1587 cm^{-1} corresponds to -N-H bending of secondary amides after forming the bond with GO. The last result indicates the presence of carboxyl and amino groups supporting a new covalent functionalization between the carboxylic acid on the GO and the amino of CS [31]. Additionally, the band corresponding to the amide group confirms bond formation between CS and GO [39].

The ^{13}C-NMR characterization was performed for CS (Figure 3) and CS-GO (Figure 4) in the solid-state as both samples were insoluble in organic solvents [40]. Full signals with some overlapping are observed, indicating loss of crystallinity when chitin is deacetylated [41]. Figure 3 showed six well-defined carbon signals comparable to those obtained by Alvarenga (2011) [42]. These signals were observed between the 27 and 110 ppm, indicating a high structural homogeneity [43]. The signal at 109.3 ppm corresponds to the anomeric carbon (C1), while a weak signal at 27.9 ppm is assigned to the methyl group (C8) of the N-acetylglucosamine. The methylene signal (C6) is observed at 64.6 ppm, while that for C2 is found at 62.6 ppm. Finally, two overlapped signals at 79.4 and 86.9 ppm corresponding to the resonance of C3 and C5 are observed [41].

The ^{13}C-NMR spectrum for CS-GO (Figure 4) is remarkably similar to the CS spectrum due to its chemical structure. Both the anomeric carbon and the methyl groups are present. A decreased methylene signal is observed, and the C5 band's displacement to 87.03 ppm is attributed to the presence of GO.

CS was characterized by Gel Permeation Chromatography (GPC) and the molecular weight (Mw) obtained was 15323 Da. CS of low molecular weight is generally considered in a range of 50–200 kDa. [44]. After the functionalization, CS-GO MW was measured, obtaining a figure of 329960 Da. This increase in MW can be attributed to the GO bonded to CS chains.

TGA analysis showed that both CS and CS-GO films presented a similar decomposition temperature. Figure 5a shows the CS thermogram, in which two significant mass losses are observed. The first loss occurs between 30-50 °C with a maximum at 33 °C, corresponding to water loss absorbed by the sample and the chitosan's weak hydrogen bonds. The second mass loss is observed between 290-396 °C with a maximum at 305 °C, where 50% of the mass is loosed. This event corresponds to the sample decomposition due to the depolymerization process [41].

The CS-GO thermogram (Figure 5b) shows a first mass loss corresponding to the water present in the sample and a second event whose range is very close to that observed for CS, with a maximum of 299 °C due to the chitosan depolymerization and pyranose rings decomposition by dehydration and deamination [41]. Additionally, it was evidenced that the CS-GO presented a lighter mass loss (~10% less loosed) than CS due probably to the GO's presence that improves thermal resistance.

On the other hand, for GO (Figure 5c), excellent-high thermal stability is observed with a low-mass loss. A slight loss of mass is observed before 100 °C, attributed to the evaporation of absorbed water and a second mass loss at 179 °C due to some oxygenated functional group decomposition. A 30% mass loss, between 150-200 °C, implies a high content of functional oxygen groups in the GO [45]. Remarkably, GO film was relatively stable to thermal analysis; also, it is interesting that the decomposition temperature occurs above the body temperature, which means that the material will be very durable for implantation.

In vitro tests were performed to analyze CS-GO biocompatibility and cell growth. A biocompatibility test was carried out with brine shrimp larvae cultured with CS-GO membranes. After 24, 36, and 48 h, live larvae were counted, and cytotoxicity percentage was calculated [46]. The toxicity of CS-GO membranes was 16%. On the other hand, a cell growth test with CS-GO membranes was carried out using gingival fibroblasts. After nine days, cells were counted, with a continual growth after cell culture. Both analyzes proved material biocompatibility and cell growth potential.

After the in vitro studies, subdermal implantation studies were carried out to observe the body's inflammatory response and, therefore, material biocompatibility/degradation. This is considered as a first approximation to determine material biocompatibility as the skin is rich

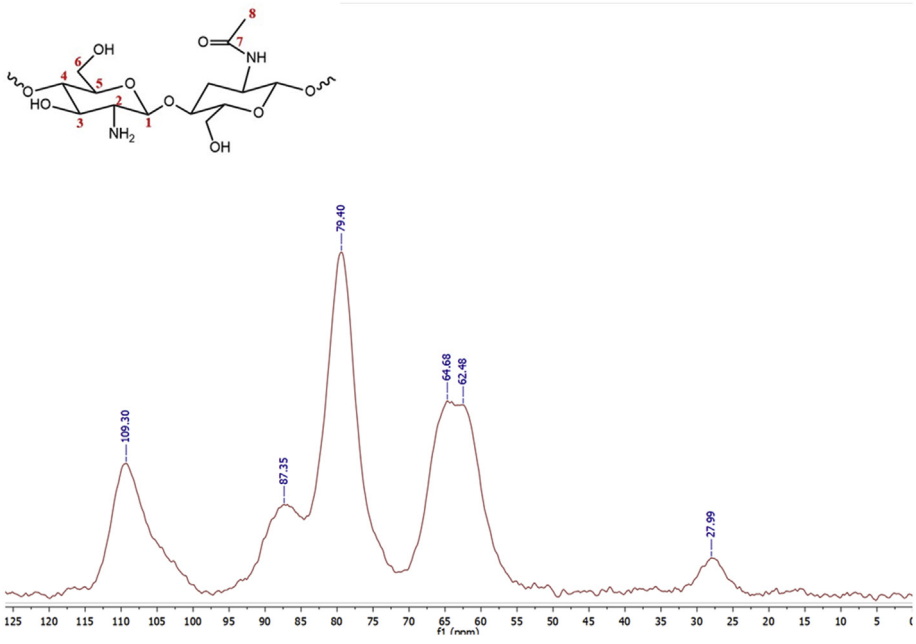

Figure 3. The solid-state ^{13}C-NMR characterization of CS.

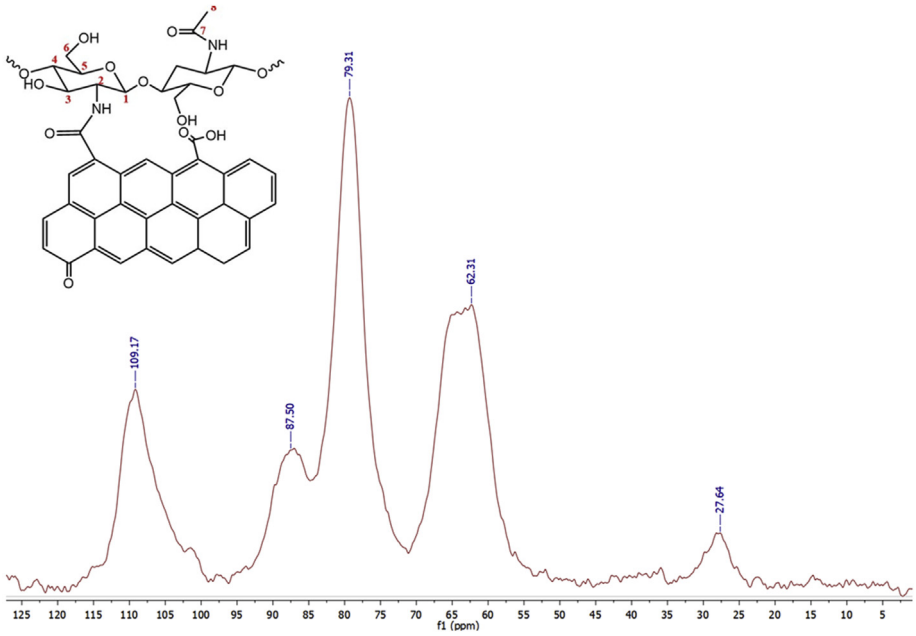

Figure 4. The solid-state ^{13}C-NMR characterization of CS-GO.

in inflammatory cells and has been used before to evaluate biomaterials [47, 48].

Histology results of implantation after 30 days are shown in Figure 6. Hair recovery and healthy skin are apparent for the biomodels. According to Sarah Al-Maawi et al. (2019), ideal cicatrization results after a surgical process with tissue recovering normal homeostasis conditions are present before surgery [49]. Implantation zone (IZ) after trichotomy is shown in Figure 6B, where dry skin, normal appearance, and presence of stitches indicate a normal cicatrization process with the absence of the necrotic zone. In Figure 6c, corresponding to a subdermal tissue, it is visible that implanted material (CS-GO) is included in the tissue and surrounded by a very transparent soft skin layer, which means that the material was successfully encapsulated with a normal cicatrization process [50].

Samples recovered from the implantation were processed by Hematoxylin and Eosin (HE) and Gomori trichrome (GT) techniques for histology studies. Figure 7 shows the collagen (control) images by both methods at 4×. Complete reabsorption of the control material (Figure 7A) can be observed with some persistence of experimental material CS-GO (Figure 7B) in the IZ. In both cases, recovery of the tissue architecture is found with the presence of continuous areas of the epidermis (E), dermis (D), and hypodermis (H).

Figure 8A shows the Gomori's trichrome technique tissue images with experimental material CS-GO at higher magnification (40×). The material is surrounded by a fibrous capsule (FC) with large blood vessels (BV). Figure 8B shows blood vessels in the middle of the material and the presence of macrophages (Mf) and histiocytes (H), which are the cells responsible for engulfing the implanted material. The previous observation means that a normal tissue cicatrization process is taking place for the implanted materials. According to Anderson (2008), granulation tissue is persistent in the implantation zone characterized by

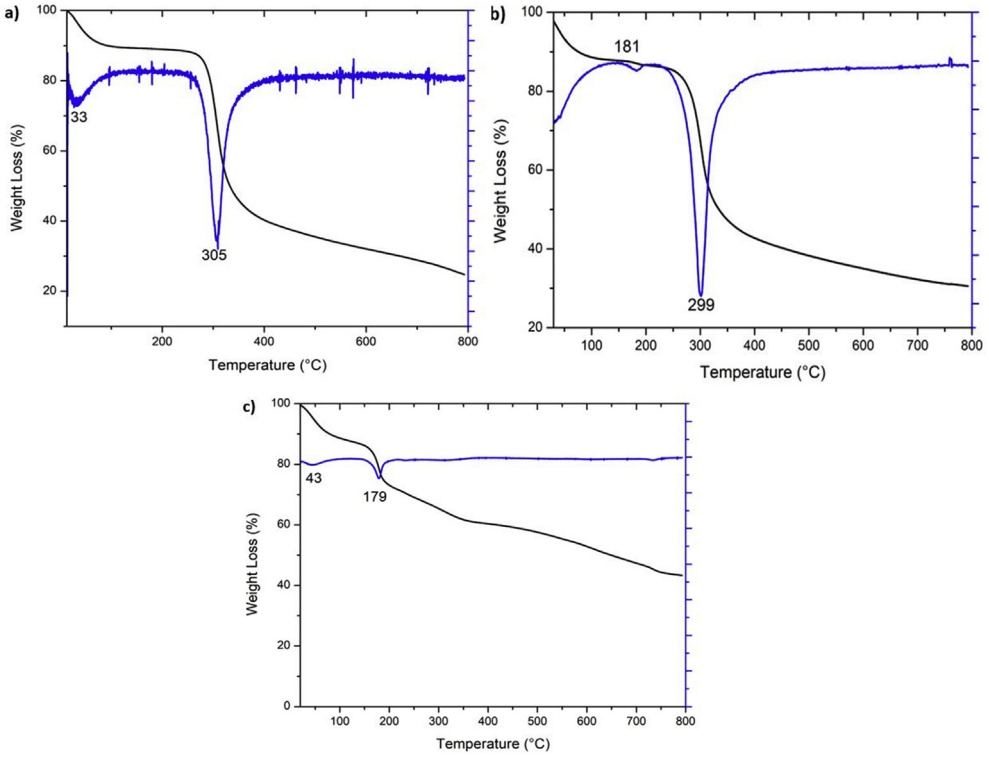

Figure 5. Thermogravimetric analysis of a) CS, b) CS-GO, and c) GO.

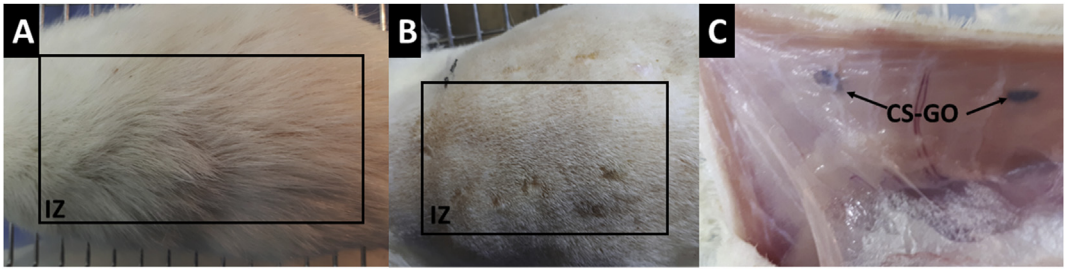

Figure 6. Macroscopic appearance of the implanted area in Wistar rat after 30 days of implantation. A. Macroscopically appearance of the skin. B. External surface of the skin. C. Internal surface of the skin. IZ: Implantation Zone. CS-GO: Chitosan-Graphene Oxide membrane.

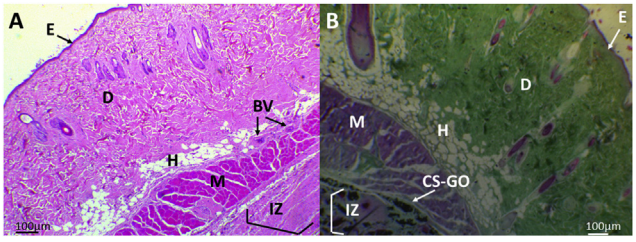

Figure 7. Microscopic images at 4× of CS-GO: Chitosan-Graphene Oxide. A. Hematoxylin-Eosin Technique. B. Gomori trichrome technique. IZ: Implantation Zone. E: Epidermis. D: Dermis. H: Hypodermis. M: Muscle.

macrophages with osteoblast and blood vessels [48], very similar at 30 days of implantation after passing the acute and chronic inflammation.

Both implanted films showed partial resorption. However, CS films (Figure 9A) showed a severe inflammatory response by Masson's trichrome technique. Meanwhile, CS-GO films (Figure 9B) showed a partial fragmentation surrounded by a fibrous capsule constituted by collagen type I, with an abundance of inflammatory cells infiltrates and a degradation/reabsorption process.

Remarkably attractive, both materials showed a fibrous capsule, which is typical in biocompatible materials; however, the CS membrane presented more significant inflammation in the implantation area.

After 60 days of implantation, tissue was completely scarred with a normal healthy macroscopic appearance for CS and CS-GO films. Microscopically, there was healthy tissue recuperation with the presence of an implantation zone containing the material in different states of degradation/reabsorption and surrounded by a fibrous capsule constituted by collagen type I and inflammatory infiltrate.

On the other hand, to analyze the biocompatibility after chemical functionalization of GO with CS as compared to the CS/GO physical mixture, histological studies with both samples were studied by Masson's trichrome technique at 4× (CS-GO, Figure 10A, and physical combination, CS/GO, Figure 10B). The implanted material corresponding to the functionalized sample presents more significant fragmentation and reabsorption than the physical mixture sample (Figure 10B). The previous result confirmed that the CS-GO showed better biological performance with a low inflammatory response and higher reabsorption than CS/GO under the same implantation conditions.

Figure 11 corresponds to Masson's trichrome technique analysis of CS-GO and CS/GO films at higher magnification (10×). It is evidenced how the functionalized sample is fragmented, and each portion has been

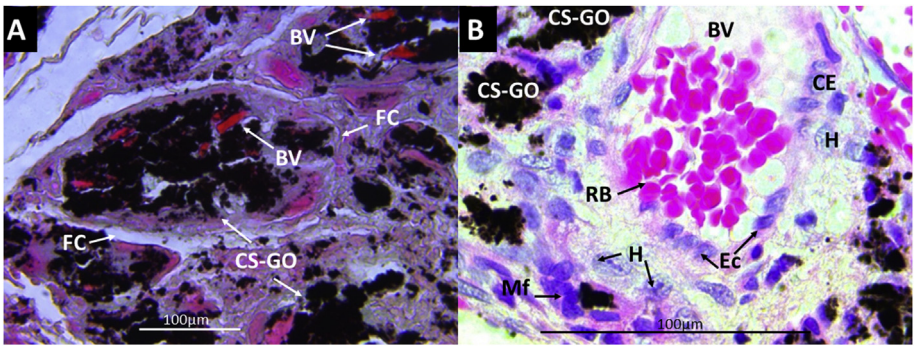

Figure 8. Gomori's trichrome technique images of CS-GO film implanted at 30 days. A. At 40×. B. At 100×. BV: Blood vessels. FC: Fibrous capsule. CS-GO: Chitosan-Graphene Oxide. RB: Red blood cells. Mf: Macrophages. H: Histiocytes.

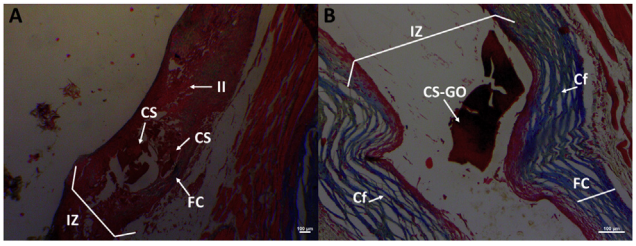

Figure 9. Masson's trichrome technique images at 10× of CS and CS-GO films implanted at 30 days. A. CS films B. CS-GO films. IZ: Implantation Zone. FC: Fibrous capsule. CS-GO: CS-GO membrane. CS: Chitosan film.

surrounded by an individual capsule composed of collagen type I. In contrast, the physical mixture (CS/GO) exhibited a lower absorption of the material.

Figure 12 corresponds to Masson's trichrome technique analysis of CS-GO and CS/GO films at 40×. The implanted zones with blood vessels necessary for the degradation/reabsorption process of implanted materials and cicatrization are evident. The presence of blood vessels is needed to transport inflammatory cells responsible for engulfing dead tissue, rests of implanted material, and to transport growth and chemotactic factors for the proliferation of repairing cells (fibroblasts) [51, 52].

All cicatrization stages are regulated by growth factors like the epidermal growth factor (EGF), which stimulates the cicatrization by numerous angiogenesis mechanisms [53]. In this research, multiple

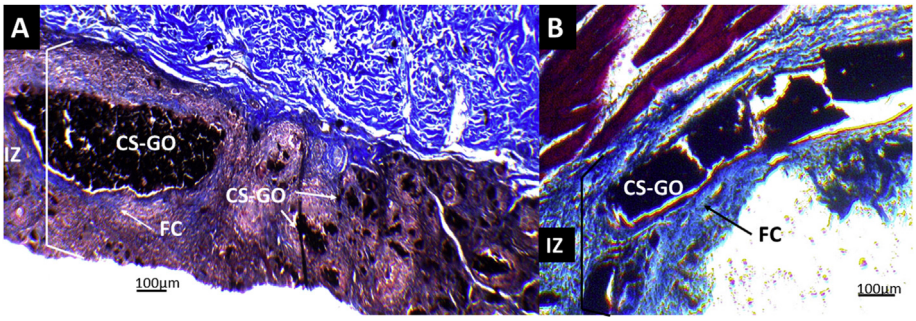

Figure 10. Masson's trichrome technique images at 4× of CS-GO and CS/GO films implanted at 60 days. A. CS-GO films. B. CS/GO films. IZ: Implantation zone. FC: Fibrous capsule. CS-GO: Chitosan-Graphene Oxide. CS/GO: Chitosan/Graphene Oxide physical mixture.

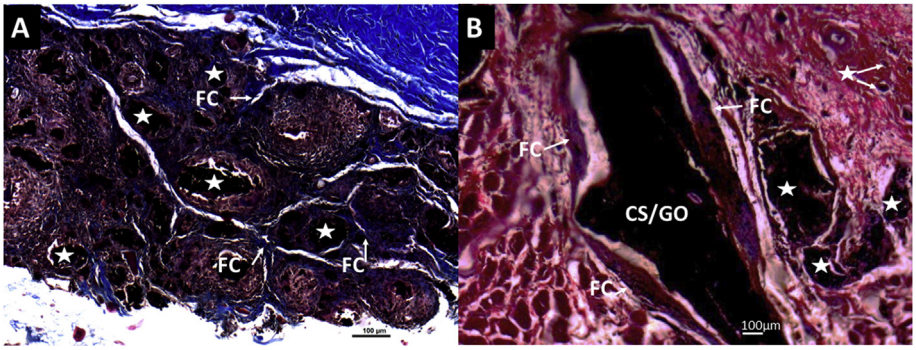

Figure 11. Masson's trichrome technique images at 10× of CS-GO and CS/GO films implanted at 60 days. A. CS-GO films. B. CS/GO films. FC: Fibrous Capsule. CS-GO: Functionalized Chitosan-Graphene Oxide. CS/GO: Chitosan/Graphene Oxide physical mixture. Stars: CS-GO fragments in the process of degradation/reabsorption.

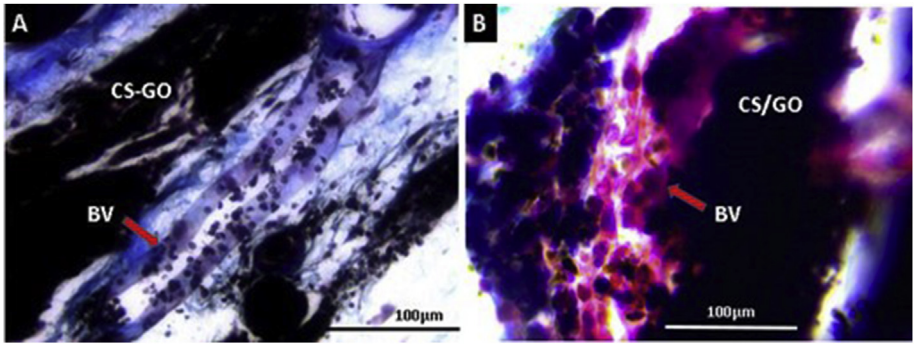

Figure 12. Masson's Trichrome Technique images at 40× of CS-GO and CS/GO films implanted at 60 days. A. CS-GO films. B. CS/GO films. BV: Blood vessel. CS-GO: Chitosan-Graphene Oxide covalently functionalized. CS/GO: Chitosan/Graphene Oxide Physical Mixture.

blood vessels in the surgical preparation zone promote a cicatrization process.

The role of blood vessels in tissue cicatrization is associated with the maintaining of the temporal matrix that is formed in each cicatrization process stage and provides the necessary support to cells responsible for creating the new tissue by giving nutrients and oxygen [53].

The cicatrization process is activated when is necessary to repair a wound, whereby the successive stages of inflammation, proliferation, and reparation are developed, followed by the formation of a scar and the tissue's recovery. However, the implantation of material produces a new situation altering the development of the stages due to the body's need to reabsorb the material by phagocytosis. In this process, the material is surrounded by a fibrous capsule [54].

A biocompatible material is expected to be surrounded by the capsule. If biodegradable, it will be resorbed, which means that the biodegradation/phagocytosis process will co-occur within a cycle with tissue recovering similar to the previous architecture before the surgical procedure lesion [49].

The present results in our research indicate that the CS-GO films might be applied in tissue engineering due to the low inflammation produced (CS and CS/GO), an essential requisite to avoid immune aggressive responses and infections.

4. Conclusions

FTIR and ^{13}C-NMR successfully demonstrated the covalent functionalization of GO with CS through an amide group formation reaction that was characterized by the presence of bands around 1600 cm^{-1} in the FTIR analysis, bands located in 1348 cm^{-1} (D band), 1593 cm^{-1} (G band), and 2416 cm^{-1} (2D band) on RAMAN, and the displacement of the signal at 87.03 ppm (C5) in solid-state ^{13}C-NMR. Films with the chitosan functionalized graphene oxide (CS-GO) were prepared and characterized by thermogravimetric analysis (TGA), where CS-GO film presented a 10% loss mass lower than CS, indicating that covalent functionalization with GO provided thermal resistance to the films. Subdermal implantation of CS and CS-GO films determined that covalent functionalization of GO with CS was fundamental to decrease the inflammatory response, as evidenced by the histological results. Better interaction with the amide groups and body fluids is probably the cause of a lower inflammatory response. Histological studies showed that CS and GO's covalent bond improved the physical and biological properties, enabling higher compatibility and faster reabsorption/degradation. The results of this investigation contributed to exhibit how the functionalization of CS-GO decreased the inflammatory response that our group has observed in previous research in which a physical mixture (CS/GO) was used. A limitation of this research is that a study performed in biomodels is not 100% transferable to human beings. For this reason, additional studies in different biomodels are required to have the authorization to continue with in-vivo studies in human beings.

Declarations

Author contribution statement

Ana María Valencia: Performed the experiments; Analyzed and interpreted the data; Wrote the paper.

Carlos Humberto Valencia: Conceived and designed the experiments; Performed the experiments; Wrote the paper.

Fabio Zuluaga: Contributed reagents, materials, analysis tools or data.

Carlos David Grande-Tovar: Conceived and designed the experiments; Analyzed and interpreted the data; Wrote the paper.

Funding statement

This research did not receive any specific grant from funding agencies in the public, commercial, or not-for-profit sectors.

Data availability statement

Data included in article/supp. material/referenced in article.

Declaration of interests statement

The authors declare no conflict of interest.

Additional information

No additional information is available for this paper.

References

[1] M.A. Nguyen, G. Camci-unal, Unconventional tissue engineering materials in disguise, Trends Biotechnol. 1–13 (2019).
[2] S. Saber-Samandari, S. Saber-Samandari, Biocompatible nanocomposite scaffolds based on copolymer-grafted chitosan for bone tissue engineering with drug delivery capability, Mater. Sci. Eng. C 75 (2017) 721–732.
[3] A. Abedi, M. Hasanzadeh, L. Tayebi, Conductive nanofibrous chitosan/PEDOT:PSS tissue engineering scaffolds, Mater. Chem. Phys. 237 (October 2018) (2019) 121882.
[4] L.A. Loureiro dos Santos, Natural polymeric biomaterials: processing and properties, Ref. Modul. Mater. Sci. Mater. Eng. (2017) 1–6.
[5] K. Balagangadharan, S. Dhivya, N. Selvamurugan, Chitosan based nanofibers in bone tissue engineering, Int. J. Biol. Macromol. 104 (2017) 1372–1382.
[6] A. Muxika, A. Etxabide, J. Uranga, P. Guerrero, K. de la Caba, Chitosan as a bioactive polymer: processing, properties and applications, Int. J. Biol. Macromol. 105 (2017) 1358–1368.
[7] S.M. Ahsan, M. Thomas, K.K. Reddy, S.G. Sooraparaju, A. Asthana, I. Bhatnagar, Chitosan as biomaterial in drug delivery and tissue engineering, Int. J. Biol. Macromol. 110 (2017) 97–109.
[8] F. Tao, Y. Cheng, X. Shi, H. Zheng, Y. Du, W. Xiang, H. Deng, Applications of chitin and chitosan nanofibers in bone regenerative engineering, Carbohydr. Polym. 230 (October 2019) (2019) 115658.
[9] J.Z. Knaul, S.M. Hudson, K.A.M. Creber, Improved mechanical properties of chitosan fibers, J. Appl. Polym. Sci. 72 (13) (1999) 1721–1732.

[10] K. Pieklarz, M. Tylman, Z. Modrzejewska, Current progress in biomedical applications of chitosan-carbon nanotube nanocomposites: a review, Mini Rev. Med. Chem. 20 (16) (2020) 1619–1632.

[11] D.C. Grande Tovar, I.J. Castro, H.C. Valencia, P.D. Navia Porras, J. Herminsul Mina Hernandez, E.M. Valencia Zapata, N.M. Chaur, Nanocomposite films of chitosan-grafted carbon nano-onions for biomedical applications, Molecules (2020).

[12] C.D. Grande Tovar, J.I. Castro, C.H. Valencia, D.P. Navia Porras, M. Hernandez, J. Herminsul, M.E. Valencia, J.D. Velásquez, M.N. Chaur, Preparation of chitosan/poly (vinyl alcohol) nanocomposite films incorporated with oxidized carbon nano-onions (Multi-Layer fullerenes) for tissue-engineering applications, Biomolecules 9 (11) (2019) 684.

[13] B. Sharma, S. Shekhar, P. Jain, R. Sharma, K.K.D. Chauhan, Graphene grafted chitosan nanocomposites and their applications, in: Graphene Based Biopolymer Nanocomposites, Springer, 2021, pp. 135–147.

[14] A. Raslan, L.S. Del Burgo, J. Ciriza, J.L. Pedraz, Graphene oxide and reduced graphene oxide-based scaffolds in regenerative medicine, Int. J. Pharm. 580 (2020) 119226.

[15] D.C. Grande Tovar, I.J. Castro, H.C. Valencia, A.P. Zapata, A.M. Solano, E. Florez López, N.M. Chaur, E.M. Valencia Zapata, H.J. Mina Hernandez, Synthesis of chitosan beads incorporating graphene oxide/titanium dioxide nanoparticles for in vivo studies, Molecules (2020).

[16] S.C. Ray, Application and Uses of Graphene Oxide and Reduced Graphene Oxide, Elsevier Inc., 2015.

[17] V. Gupta, N. Sharma, U. Singh, M. Arif, A. Singh, Higher oxidation level in graphene oxide, Optik 143 (2017) 115–124.

[18] A.T. Smith, A.M. LaChance, S. Zeng, B. Liu, L. Sun, Synthesis, properties, and applications of graphene oxide/reduced graphene oxide and their nanocomposites, Nano Mater. Sci. 1 (1) (2019) 31–47.

[19] B. Yang, P.-B. Wang, N. Mu, K. Ma, S. Wang, C.-Y. Yang, Z.-B. Huang, Y. Lai, H. Feng, G.-F. Yin, Graphene oxide-composited chitosan scaffold contributes to functional recovery of injured spinal cord in rats, Neural Regen. Res. 16 (9) (2021) 1829.

[20] C. Xie, X. Lu, L. Han, J. Xu, Z. Wang, L. Jiang, K. Wang, H. Zhang, F. Ren, Y. Tang, Biomimetic mineralized hierarchical graphene oxide/chitosan scaffolds with adsorbability for immobilization of nanoparticles for biomedical applications, ACS Appl. Mater. Interfaces 8 (3) (2016) 1707–1717.

[21] H. Yi, L.Q. Wu, W.E. Bentley, R. Ghodssi, G.W. Rubloff, J.N. Culver, G.F. Payne, Biofabrication with chitosan, Biomacromolecules 6 (6) (2005) 2881–2894.

[22] F. Saeedi, A. Montazeri, Y. Bahari, M. Pishvaei, B. Jannat, M. Rasa, F. Saeedi, Fabrication and characterization of chitosan-polyvinyl alcohol-graphene oxide nanocomposite scaffold for wound healing purposes, Human, Heal. Halal Metrics 1 (2) (2021) 47–55.

[23] N. Amiryaghoubi, M. Fathi, A. Barzegari, J. Barar, H. Omidian, Y. Omidi, Recent advances in polymeric scaffolds containing carbon nanotube and graphene oxide for cartilage and bone regeneration, Mater. Today Commun. (2021) 102097.

[24] P.P. Zuo, H.F. Feng, Z.Z. Xu, L.F. Zhang, Y.L. Zhang, W. Xia, W.Q. Zhang, Fabrication of biocompatible and mechanically reinforced graphene oxide-chitosan nanocomposite films, Chem. Cent. J. 7 (1) (2013) 1–11.

[25] D.L. Tenorio, C.H. Valencia, C. Valencia, F. Zuluaga, M.E. Valencia, J.H. Mina, C.D.G. Tovar, Evaluation of the biocompatibility of Cs-graphene oxide compounds in vivo, Int. J. Mol. Sci. 20 (7) (2019).

[26] C. Valencia, C.H. Valencia, F. Zuluaga, M.E. Valencia, J.H. Mina, C.D. Grande-Tovar, Synthesis and application of scaffolds of chitosan-graphene oxide by the freeze-drying method for tissue regeneration, Molecules 23 (10) (2018).

[27] S. Biranje, P. Madiwale, A.R.V. Adicarekar, Preparation and characterization of chitosan/pva polymeric film for its potential application as wound dressing, Material. *Indian J.Sci. Res* 14 (2) (2017) 250–256.

[28] T. Ramanathan, A.A. Abdala, S. Stankovich, D.A. Dikin, M. Herrera-Alonso, R.D. Piner, D.H. Adamson, H.C. Schniepp, X. Chen, R.S. Ruoff, S.T. Nguyen, I.A. Aksay, R.K. Prud'Homme, L.C. Brinson, Functionalized graphene sheets for polymer nanocomposites, Nat. Nanotechnol. 3 (6) (2008) 327–331.

[29] S.H.M. Wong, S.S. Lim, T.J. Tiong, P.L. Show, H.F.M. Zaid, H.-S. Loh, Preliminary in vitro evaluation of chitosan–graphene oxide scaffolds on osteoblastic adhesion, proliferation, and early differentiation, Int. J. Mol. Sci. 21 (15) (2020) 5202.

[30] L. Carson, C. Kelly-Brown, M. Stewart, A. Oki, G. Regisford, Z. Luo, V.I. Bakhmutov, Synthesis and characterization of chitosan-carbon nanotube composites, Mater. Lett. 63 (6–7) (2009) 617–620.

[31] Snežzana Miljanić, Leo Frkanec, Tomislav Biljan, Zlatko Meić Mladen Žini, Recent advances in linear and nonlinear Raman spectroscopy I, J. Raman Spectrosc. 38 (April) (2007) 1538–1553.

[32] D.C. Marcano, D.V. Kosynkin, J.M. Berlin, A. Sinitskii, Z. Sun, A. Slesarev, L.B. Alemany, W. Lu, J.M. Tour, Improved synthesis of graphene oxide, ACS Nano 4 (8) (2010) 4806–4814.

[33] D. López-Díaz, M. López Holgado, J.L. García-Fierro, M.M. Velázquez, Evolution of the Raman spectrum with the chemical composition of graphene oxide, J. Phys. Chem. C 121 (37) (2017) 20489–20497.

[34] D. Ma, X. Li, Y. Guo, Y. Zeng, Study on IR properties of reduced graphene oxide, IOP Conf. Ser. Earth Environ. Sci. 108 (2) (2018).

[35] Y. Pan, T. Wu, H. Bao, L. Li, Green fabrication of chitosan films reinforced with parallel aligned graphene oxide, Carbohydr. Polym. 83 (4) (2011) 1908–1915.

[36] K.S.S.K. Muhamad, F. Mohamed, S. Radiman, A. Hamzah, S. Sarmani, K.K. Siong, M.S. Yasir, I.A. Rahman, N.R.A.M. Rosli, Synthesis and characterization of exfoliated graphene oxide, AIP Conf. Proc. (2016) 1784.

[37] D. Han, L. Yan, W. Chen, W. Li, Preparation of chitosan/graphene oxide composite film with enhanced mechanical strength in the wet state, Carbohydr. Polym. 83 (2) (2011) 653–658.

[38] M.S. Muda, A. Kamari, S.A. Bakar, S.N.M. Yusoff, I. Fatimah, E. Phillip, S.M. Din, Chitosan-graphene oxide nanocomposites as water-solubilising agents for rotenone pesticide, J. Mol. Liq. 318 (2020) 114066.

[39] W.F. Khalil, G.S. El-Sayyad, W.M.A. El Rouby, M.A. Sadek, A.A. Farghali, A.I. El-Batal, Graphene oxide-based nanocomposites (GO-Chitosan and GO-EDTA) for outstanding antimicrobial potential against some Candida species and pathogenic bacteria, Int. J. Biol. Macromol. 164 (2020) 1370–1383.

[40] C. Qin, H. Li, Q. Xiao, Y. Liu, J. Zhu, Y. Du, Water-solubility of chitosan and its antimicrobial activity, Carbohydr. Polym. 63 (3) (2006) 367–374.

[41] G. Muñoz, C. Valencia, N. Valderruten, E. Ruiz-Durántez, F. Zuluaga, Extraction of chitosan from Aspergillus Niger mycelium and synthesis of hydrogels for controlled release of betahistine, React. Funct. Polym. 91–92 (June) (2015) 1–10.

[42] E.S. Alvarenga, Characterization and properties of chitosan, Biotechnol. Biopolym. (2011) 91–108.

[43] I. Younes, S. Hajji, V. Frachet, M. Rinaudo, K. Jellouli, M. Nasri, Chitin extraction from shrimp shell using enzymatic treatment. Antitumor, antioxidant and antimicrobial activities of chitosan, Int. J. Biol. Macromol. 69 (2014) 489–498.

[44] A.B. Muley, S.A. Chaudhari, K.H. Mulchandani, R.S. Singhal, Extraction and characterization of chitosan from prawn shell waste and its conjugation with cutinase for enhanced thermo-stability, Int. J. Biol. Macromol. 111 (2018) 1047–1050.

[45] P.G. Ren, D.X. Yan, X. Ji, T. Chen, Z.M. Li, Temperature dependence of graphene oxide reduced by hydrazine hydrate, Nanotechnology 22 (5) (2011).

[46] P. de A. Sarmento, T. da R. Ataíde, A.P. de S. Pinto, J.X. de Araújo-Júnior, I.M.L. Lúcio, M.L. de A. Bastos, Avaliação do extrato da zeyheria tuberculosa Na perspectiva de Um produto para cicatrização de Feridas, Rev. Lat. Am. Enfermagem 22 (1) (2014) 165–172.

[47] M. Jannasch, T. Weigel, L. Engelhardt, J. Wiezoreck, S. Gaetzner, H. Walles, T. Schmitz, J. Hansmann, In vitro chemotaxis and tissue remodeling assays quantitatively characterize foreign body reaction, ALTEX 34 (2) (2017) 253–266.

[48] M. Tomida, K. Nakano, S. Matsuura, T. K, Comparative examination of subcutaneous tissue reation to high molecular materials in medical use, Eur. J. Med. Res. (2011) 249–252.

[49] S. Al-Maawi, C. Mota, A. Kubesch, C. James Kirkpatrick, L. Moroni, S. Ghanaati, Multiwell three-dimensional systems enable in vivo screening of immune reactions to biomaterials: a new strategy toward translational biomaterial research, J. Mater. Sci. Mater. Med. 30 (6) (2019) 1–6.

[50] J.M. Anderson, A. Rodriguez, D.T. Chang, Foreign body reaction to biomaterials, Semin. Immunol. 20 (2) (2008) 86–100.

[51] D.S. Steinbrech, M.T. Longaker, B.J. Mehrara, P.B. Saadeh, G.S. Chin, R.P. Gerrets, D.C. Chau, N.M. Rowe, G.K. Gittes, Fibroblast response to hypoxia: the relationship between angiogenesis and matrix regulation, J. Surg. Res. 84 (2) (1999) 127–133.

[52] P. Kumar, S. Kumar, E.P. Udupa, U. Kumar, P. Rao, T. Honnegowda, Role of angiogenesis and angiogenic factors in acute and chronic wound healing, Plast. Aesthetic Res. 2 (5) (2015) 243.

[53] S.M. Sari Kiliçaslan, Ş. Coşkun Cevher, E.G. Güleç Peker, Ultrastructural changes in blood vessels in epidermal growth factor treated experimental cutaneous wound model, Pathol. Res. Pract. 209 (11) (2013) 710–715.

[54] M.R. Major, V.W. Wong, E.R. Nelson, M.T. Longaker, G.C. Gurtner, The foreign body response: at the interface of surgery and bioengineering, Plast. Reconstr. Surg. 135 (5) (2015) 1489–1498.